Zircon petrochronology reveals the timescale and mechanism of anatectic magma formation

Federico Farina[1], Andrea Dini[2], Joshua H.F.L.Davies[1], Maria Ovtcharova[1], Nicolas D. Greber[1], Anne-Sophie Bouvier[3], Lukas Baumgartner[3], Alexey Ulianov[3], Urs Schaltegger[1]

1: Department of Earth Sciences, University of Geneva, Switzerland
2: Instituto di Geoscienze e Georisorse, CNR, Pisa, Italy
3: Institute ofEarth Sciences, University of Lausanne, Switzerland

Abstract

Igneous rocks of intermediate to acidic composition commonly exhibit considerable degrees of isotope variability preserved at the crystal and sub-crystal scale, as well as a significant U-Pb age range, reflecting protracted timescales of zircon crystallization and long magma residence times. The association of high-precision U-Pb zircon dates with stable and radiogenic isotope data represents a powerful tool to unravel the petrological evolution of granitic rocks, hence allowing a better understanding of the processes that led to the formation and reworking of the continental crust. In this case study, we combine high-precision U-Pb dates with stable and radiogenic isotope data from zircon crystals in the Larderello-Travale (Italy) shallow-level granites. These rocks are peraluminous two-mica, cordierite-bearing granites and represent pure crustal anatectic magmas, generated in a post-collisional extensional setting. As such, they are ideal candidates to investigate the timing, rates and mechanisms of melt production during anatectic magma formation, giving insights into the process of intracrustal differentiation. Magmatic zircon crystals from the Larderello-Travale granites contain $\delta^{18}O$ values ranging from 8.6 to 13.5‰ and crystals from individual samples exhibit inter- and intra-grain oxygen isotope variability exceeding 3‰. The analysed crystals have εHf values ranging between −7.4 and −12.4, with moderate, intra-sample εHf isotope variability. All CA-ID-TIMS (chemical abration isotope-dilution thermal ionization mass spectrometry) $^{206}Pb/^{238}U$ zircon ages range from 4.5 to 1.6 Ma and suggest four pulses of magmatic activity at around 3.6, 3.2, 2.7 and 1.6 Ma. More importantly, zircon crystals from individual samples typically exhibit an age spread as large as 300-500 ka. This age dispersion suggests that most of the zircon did not crystallize at the emplacement level but in the middle crust and were subsequently recycled and juxtaposed during ascent and emplaced at shallow level. When plotted against age, stable and radiogenic isotope data suggest the co-existence of multiple and isotopically distinct magma batches produced by partial melting of different crustal domains. This requires coeval magma batches that are physically separated and evolve independently for hundreds of thousands of years before coalescing during ascent and emplacement. The involvement of multiple sources in the production of crustal anatectic magmas reflects the inherent heterogeneous nature of the continental crust and result from the interplay between the rise and evolution of the geotherms through the crust and the composition of the fertile source rocks. Finally, the isotopically diverse zircon-bearing magma batches mixed and assembled into shallow-level intrusions generated during the four major magma pulses.

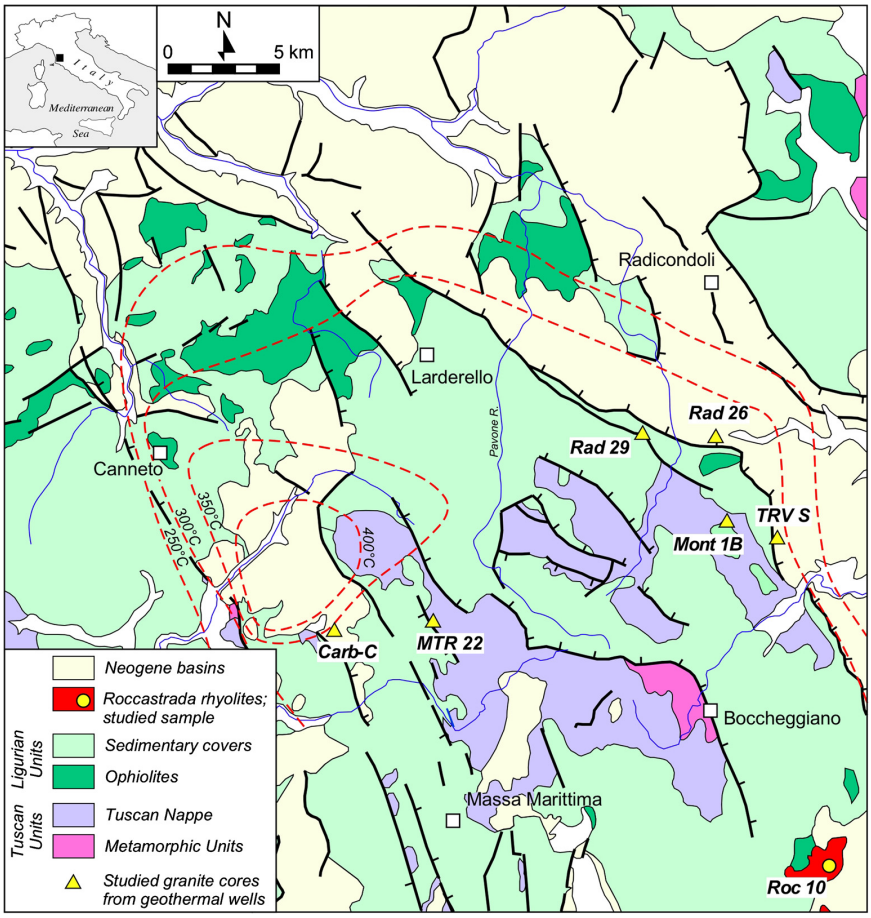

Figure 1. Geological map of the Larderello–Travale area and location of the six wells where granite core samples were collected. Red dashed lines indicate the temperature (in °C) at 3 km below the surface.

1. Introduction

In the continental crust, magmas with broadly granitic composition are formed by partial melting of a variety of different sources under water-fluxed and fluid-absent melting conditions (Brown, 2013). The removal of granitic magmas from middle and deep crustal levels and their emplacement at shallower depths has shaped the structure of the crust, enriching its upper part in incompatible and heat-producing elements and leaving its lower portion relatively mafic and refractory (Petford et al., 2000). Although crustal reworking (i.e. melting of pre-existing crustal rocks) followed by melt extraction, ascent and granite emplacement is the main agent that caused the chemical differentiation of the continental crust, the timescale of melt production and the processes controlling the chemical composition of crustally-derived granites are still poorly constrained (e.g. Clemens and Stevens, 2012).

In the last decade, the increased utilization of spatially resolved isotope analyses in igneous petrology has revealed that granitoid rocks are far less homogeneous than previously thought and are commonly characterized by large degrees of small-scale isotopic variability (Wotzlaw et al., 2014; Farina et al., 2014a, 2014b). Also, the achievement of unparalleled high-precision in CA-ID-TIMS zircon geochronology (i.e. better than 0.1% on ^{238}U–^{206}Pb dates; Schaltegger et al., 2015) has shown the common occurrence of significant U-Pb age scatter in populations of zircon crystals from individual samples of granitoids and felsic volcanic rocks (Wotzlaw et al., 2013; Barboni and Schoene, 2014; Sampertonet al., 2015). This new generation of high spatial resolution isotopic data and bulk-grain high-precision U-Pb dates has strongly contributed to the emerging view that magma reservoirs are incrementally built regions in the crust where melt, crystals, and volatiles are heterogeneously distributed in space and time (Cashman et al., 2017). The vast majority of these studies are focussed on granitoids and felsic volcanic rocks that were formed in continental and oceanic arcs and in within-plate continental settings (Wotzlaw et al., 2014; Samperton et al., 2015; Schmittet al., 2017), where felsic igneous rocks are mostly produced by mixing between mantle- and crustally-derived magmas (e.g. Szymanowski et al., 2015). Less attention has been paid to the genesis of felsic rocks originating from direct melting of pre-existing crustal material, even though from the end of the Archean such processes are predicted to have been important (Hawkesworth et al., 2018). To gain a comprehensive understanding of processes leading to the internal reworking of the continental crust, we investigated the Plio-Pleistocene shallow-level peraluminous granites from the Larderello-Travale intrusive system (Tuscany, Italy; Fig.1), which represent crustal anatectic magmas (Dini et al., 2005). We use high precision CA-ID-TIMS zircon dating combined with stable and radiogenic zircon isotope data to shed light on the rates and mechanisms of melt production as well as on the processes that generate the chemical variability observed in many S-type granitoids. Ultimately, these data will help to better understand the formation and evolution of the upper continental crust.

2. The Larderello-Travale magmatic system

The development of the northern Apennine orogenic wedge culminated at the Oligocene-Miocene boundary and was followed by widespread lithosphere extension and asthenosphere upwelling caused by the rollback and delamination of the Adriatic microplate below the European margin (Malinverno and Ryan, 1986). From

Miocene to Present, post-collisional extensional tectonics led to the opening of a continental back-arc basin (i.e. the northern Tyrrhenian Sea) and to the emplacement and eruption of rocks of the Tuscan Magmatic Province (Lustrino et al., 2011). The igneous rocks of this province are exposed across an area of about 30,000 km^2 and exhibit a significant range in composition from peraluminous anatectic products to rocks showing calc-alkaline, high-K calc-alkaline, potassic, ultrapotassic and lamproitic affinities (Lustrino et al., 2011).

In southern Tuscany, granitic intrusive bodies with Pliocene to Pleistocene ages (3.8-1.3 Ma) have been found in boreholes at 3-4 km depth (Fig.1) below the Larderello geothermal area (Dini et al., 2005; Villa et al., 2006). In this area, the thinned continental crust (~23 km) is characterised by very high heat flow with average regional values of 100-150 mW/m^2 (Gianelli et al., 1997). In the central area of the Larderello-Travale system, seismic reflection data show a continuous bright spot level at depths of 3-5 km below the surface, the so-called K-horizon (Bertini et al., 2006). Although the geological meaning of this horizon is still highly debated (Agostinetti et al., 2017), very high temperatures are observed at its top (>450°C), which suggests that the magmatic system is still active and that new magmas were recently emplaced below the Pliocene-Pleistocene granitoids.

The Larderello-Travale igneous complex is composed of high-silica monzo-and syenogranites displaying a high degree of textural and mineralogical variability. Most of these rocks are two-mica granites, containing cordierite and, more rarely, other Al-rich phases such as andalusite and dumortierite. Apatite, zircon, monazite, U-rich thorite and ilmenite are ubiquitous accessory minerals. The boron-rich character of these granites is highlighted by the ubiquitous occurrence of late-magmatic tourmaline. All the granites are highly peraluminous with alumina saturation index (i.e. molar ratio of $Al_2O_3/(CaO+Na_2O+K_2O)$) ranging between 1.10 and 1.25, and silica contents between 69 and 79wt%. The granites have high and variable initial $^{87}Sr/^{86}Sr$ whole-rock compositions (0.715-0.721) and low ε_{Nd} values spanning between −8 and −11 (Dini et al., 2005). These features indicate that the Larderello-Travale granitoids are crustal anatectic magmas that, according to Dini et al.(2005), were formed through biotite and/or muscovite fluid-absent partial melting of aluminous metasediments. The age of the granites ranges between 3.8 Ma (biotite K-Ar age) and 1.3Ma (muscovite ^{39}Ar-^{40}Ar), with a few ^{39}Ar-^{40}Ar muscovite and biotite samples also yielding ages between 2.5-2.25 Ma (Dini et al., 2005).

3. Workflow and analytical methods

To investigate the petrogenesis of the Larderello-Travale magmatic system, we conducted high-precision CA-ID-TIMS U-Pb dating combined with oxygen and hafnium isotope analyses of zircon crystals from six monzogranite core samples. Four of the sampled wells are from the eastern part of the geothermal field, while the other two are located 5-10 km westward, close to the area characterized by the highest thermal anomaly in the geothermal field (Fig.1). Five out of six samples are from depths between 4100 and 4300 m, while sample Mont-1B was drilled at ~3100 m. The petrography and whole-rock geochemistry of four of the samples (i.e. Rad-29, Rad-26, Carb-C, TRV-S) is described in Dini et al. (2005), while the other two samples (MTR-22 and Mont 1B) have not been studied in detail.

To determine the petrogenesis of the Larderello-Travale granites, we implemented an analytical workflow integrating in-situ and bulk-grain zircon analysis. The workflow consists of five steps: i)zircon imaging by cathodoluminescence; ii)oxygen isotope ($\delta^{18}O$) determination by Secondary Ion Mass Spectrometry (SIMS) from specific zones in the core and rim of the grains; iii) in-situ U-Pb dating performed by laser ablation-inductively coupled plasma mass spectrometry (LA-ICP-MS) on inherited cores; iv) CA-ID-TIMS U-Pb geochronology on selected grains that had previously been analysed for their oxygen isotopic composition; v) bulk-grain solution Hf isotope measurements by multi-collector inductively coupled plasma mass spectrometry (MC-ICP-MS) performed on zircon washes from U-Pb geochronology.

CA-ID-TIMS U-Pb zircon dates were also determined for zircon crystals from one rhyolite sample of the Roccastrada volcanic complex (sample Roc-10), cropping out ~10 km south of the geothermal field. These lavas are distributed over an area of ~100km^2 and have chemical and isotopic compositions similar to the granites of the Larderello-Travale system (Pinarelli et al., 1989), which suggests a petrogenetic kinship between the lavas and the shallow-level granitoids.

A complete description of the analytical methods is provided as Supplementary material together with complete documentation of the analysed crystals (Tables S1-S6, Figs. S1-S2). Our database includes thirty-three zircon grains for which CL-images, high-precision U-Pb ages, oxygen and Hf isotope data have been collected (Table S6 in the Supplementary material).

4. Results

4.1. Zircon textures

Zircon crystals from the Larderello-Travale granites and Roccastrada rhyolite are mostly prismatic or stubby. Crystal lengths range from 50 to 400μm and aspect ratios (i.e. length/width) from 2:1 to 5:1. The zoning pattern of ~1000 zircon grains from the seven samples was characterized under cathodoluminescence(CL hereafter). Despite the large textural variability exhibited, the zircon grains can be grouped into five types ranging from relatively simple textures (types 1, 2 and 3) to complex grains (types 4, 5). These are:

1. Grains with well-developed pyramid shape (211) showing fine-scale oscillatory and sector zoning. Some of these crystals contain small (10-15μm), sub-rounded, homogeneous centres with bright CL characteristics (Fig.2).
2. Grains showing core-to-rim oscillatory zoning. A few crystals of this group contain perfect concentric zonation, others contain two different growth zones that are not separated by resorption surfaces (Fig.2).
3. Grains with featureless or faintly-zoned centres. The centres are most commonly CL-bright surrounded by fine-scale oscillatory zoned rims (Fig.2).
4. Grains exhibiting centres with convoluted zoning and irregular CL-dark patterns commonly overgrown by oscillatory zoned or dark rims (Fig.2). In many crystals, the convoluted zoning in the centre overprints partially-preserved oscillatory zoning.
5. Euhedral zircon grains exhibiting sub-rounded oscillatory zoned and/or homogeneous centres overgrown by oscillatory zoned rims. The contact between the centre and the surrounding rim is irregular and sometimes highly lobate. Thin irregular areas at the core-rim boundary that show transgressive recrystallization are also relatively common. In some cases, the centres display an internal zoning that is truncated by the zoning in the rim and/or have a morphology that is substantially different from the external morphology of the crystal. In these cases, the centres are interpreted as inherited cores (Fig.2).

The proposed classification is qualitative and the attribution of a given crystal to one of the textural type described above is not always straightforward. In fact, it is not uncommon to have

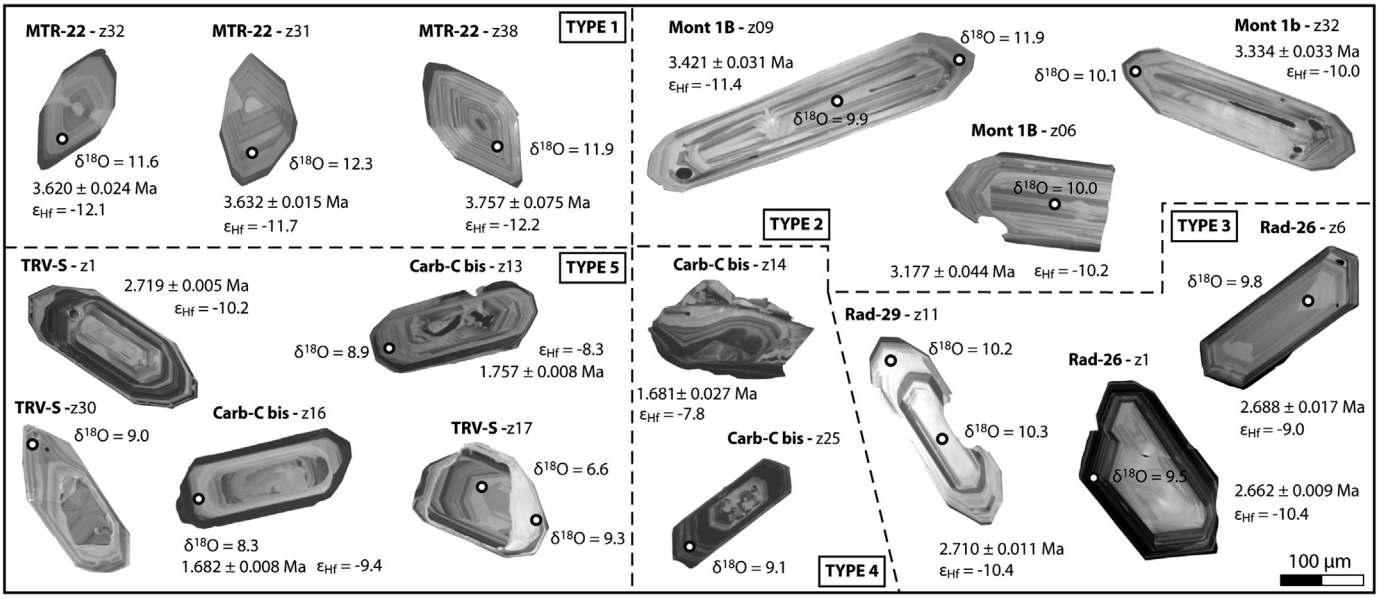

Figure 2. Cathodoluminescence images of zircon crystals from the Larderello–Travale granites and Roccastrada rhyolites. Individual oxygen isotope spots are shown by white circles, and corresponding $^{206}Pb/^{238}U$ ages and Hf isotopic compositions are placed below each grain.

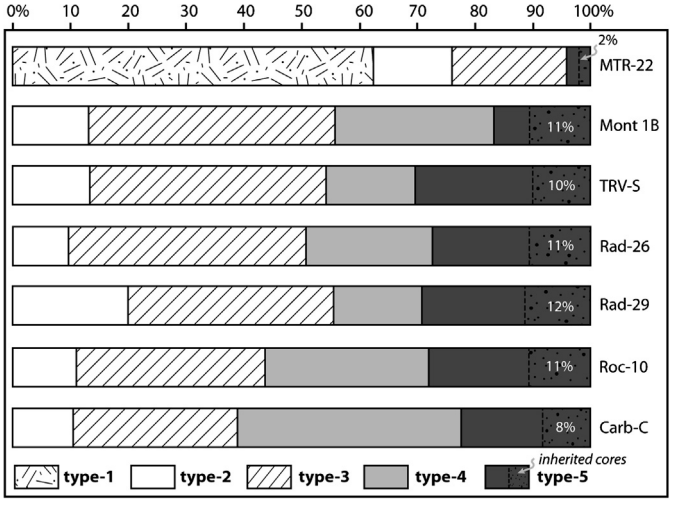

Figure 3. Frequency diagram showing the distribution of the different zircon types recognized by cathodoluminescence. For each sample, the percentage of zircon Grains having an inherited core has been estimated based on CL images and a reconnaissance LA–ICP–MS U–Pb survey.

crystals without a clear-cut affinity to one of these types or crystals whose internal structure could fit into more than one of the groups. In spite of this complication, a few significant differences among the samples emerge from the frequency histogram of Fig.3, which shows the relative abundance of the five zircon textures. Type–1 zircon grains are characteristic of sample MTR–22, constituting ~60% of the entire zircon population while, this zircon–type is absent in all the other samples. Grains with centres characterized by convoluted zoning (type–4) are abundant in sample Carb–C (~40%). Finally, samples Mont 1B, Rad–26, Rad–29, TRV–S as well as the rhyolite (Roc–10) have a similar distribution of zircon textures, with types 4 and 5 textures representing between 50 and 70% of the total zircon grains, respectively.

4.2. U–Pb LA–ICP–MS on inherited cores

One hundred spot analyses were performed on partially resorbed zircon centres. Of these, only twenty–six were inherited cores. Only eighteen analyses were sub–concordant passing a <10% discordancy test. The sub–concordant analyses yield apparent spot ages that vary from 129 to 2191 Ma but are dominated by Neoproterozoic and Paleozoic ages (Fig.S1 in Supplementary material and Table S2). Based on a relatively small dataset of zircon core ages, the age distribution contains peaks at c. 600, 420 and 300Ma, which is in agreement with the main peaks in the distribution of detrital zircon ages observed from metasedimentary rocks of the Tuscan basement (Paoli et al., 2016).

4.3. Oxygen isotopes

A total of 118 in–situ zircon oxygen analyses were performed on 88 grains (Table S3). The grains exhibit a range in $\delta^{18}O$ from 5.6 to 13.5‰. However, in each sample, the lowest $\delta^{18}O$ values were always measured in inherited cores (Fig.4). Excluding the inherited cores, the whole population of zircon crystals show variability in $\delta^{18}O$ of ~5‰, ranging from 8.3 to 13.5‰. Zircon crystals from individual samples also exhibit $\delta^{18}O$ inter–grain variability of greater than 3‰; an order of magnitude larger than the reproducibility obtained for the Temora–2 reference material (i.e. 0.28‰, 2SD). Significant intra–grain oxygen isotope variability is also observed. In fact, only four of the seventeen magmatic core–rim pairs have uniform oxygen isotope compositions, while the others show intra–grain $\delta^{18}O$ variations of up to 2.4‰. However, systematic differences between magmatic cores and overgrowths are not apparent as cores can be both higher or lower in their $\delta^{18}O$ values compared to the overgrowth (Fig.4).

Nineteen out of twenty–two spot analyses performed on zircon crystals from sample MTR–22 display a limited range in oxygen isotope composition, between 11.6 and 12.7 ‰ (Fig.4). The mean oxygen isotope composition calculated for magmatic zircon from sample MTR–22 is 11.9 ±0.4 ‰ (1 SD); this is the highest average $\delta^{18}O$ value determined for the zircon of the Larderello–Travale granites. Zircon grains from sample Mont 1B have $\delta^{18}O$ values ranging between 8.1 and 11.9 ‰, with 75% of analyses giving values between 9.6 and 10.7 ‰ (Fig.4). Two centres yield values of 8.1 and 9.0 ‰ and based on CL images are tentatively interpreted as inherited cores. The zircon $\delta^{18}O$ values of sample TRV–S are extremely heterogeneous, ranging from ~9 to 13.5‰ and exhibiting four clusters (Fig.4). In sample Rad–26, two spot analy–

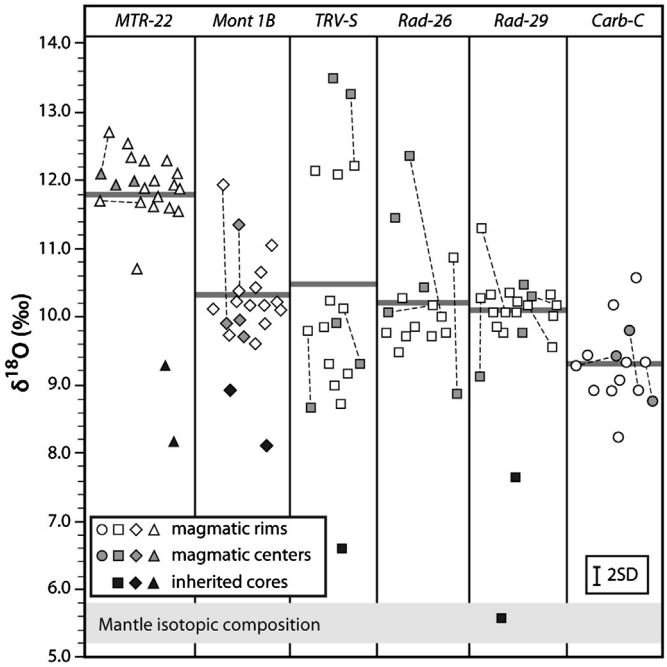

Figure 4. $\delta^{18}O$ compositions of zircon crystals from the Larderello–Travale granites. In-situ $\delta^{18}O$ composition of zircon inherited cores, magmatic centres and overgrowths. Dashed tie-lines indicate in-situ $\delta^{18}O$ analyses performed on core-rim pairs. Horizontal grey bars are $\delta^{18}O$ average values calculated for the different samples. Mantle zircon oxygen isotope composition is from Valley et al. (1998).

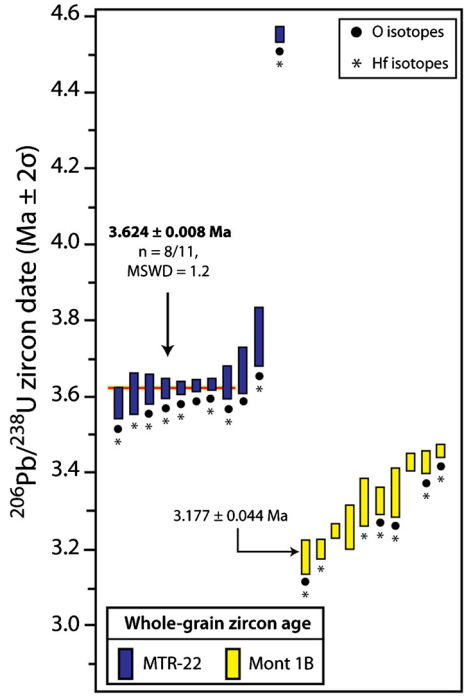

Figure 5. Rank-order plot of high-precision ID-TIMS $^{206}Pb/^{238}U$ zircon dates from two monzogranites from the Larderello–Travale intrusive system. Coloured rectangles are single-grain analyses with vertical lengths corresponding to 2σ uncertainties. Below the rectangles, asterisks indicate zircon grains for which bulk-grain Hf isotope were determined while black dots mark grains for which in-situ zircon oxygen analyses are available. For sample MTR22, the horizontal bar represents the weighted mean calculated for a cluster of eight statistically equivalent ages. The age of the youngest dated grains is indicated for sample Mont 1B.

ses performed on CL-bright centres show $\delta^{18}O$ values of 11.5 and 12.4‰. The remaining thirteen analyses yield lower isotopic values ranging between 8.9 and 10.9 ‰. Magmatic zircon from sample Rad-29 yields a mean isotopic composition of 10.1 ± 0.4‰ (1 SD) with ~70% of analyses between 10.0 and 10.5‰. The oxygen isotope composition of two inherited cores were also analysed, these have $\delta^{18}O$ values of 5.6 and 7.7‰. Finally, in sample Carb-C, magmatic zircon yields the lowest mean oxygen isotope composition (9.3 ±0.6‰ ;Fig.4), with values ranging between 8.3 and10.6‰.

4.4. CA-ID-TIMS U-Pb zircon geochronology

A total of 99 single zircon crystals from the six monzogranites and the Roccastrada rhyolite have been dated by CA-ID-TIMS (Figs.5and 6). All $^{206}Pb/^{238}U$ zircon dates were corrected for initial $^{230}Th-^{238}U$ disequilibrium as described in the Supplementary material. Zircon U-Pb ages in the granites span between ~4.5 and 1.6 Ma and have a mean 2σ analytical precision of ±0.03 Ma on individual zircon analyses. The geochronological data reveal the occurrence of four main pulses of magmatic activity. The oldest and the youngest magmatic pulses are from the western part of the complex. Sample MTR-22 contains zircon crystals with ages ranging predominantly between 3.7 and 3.6 Ma while at the same depth and two km eastward, the youngest magmatic pulse (sample Carb-C) contains grains with ages between 2.0 and 1.7 Ma (Figs.5, 6). In the eastern part of the complex, the monzogranite Mont 1B, contains the oldest grains, with zircon crystals ranging in age from 3.4 to 3.2 Ma (Mont 1B, Fig.5). In the same area, the other three monzogranites (samples Rad-29, Rad-26, TRV-S, Fig.6) have zircon age variability mostly falling in the 2.9–2.6Ma range. Zircon grains from the Roccastrada rhyolite also share this age variability (Roc-10, Fig.6). It is worth noting that the oldest monzogranite from the eastern magmatic pulse (i.e. Mont 1B) was collected from a depth of 3000m, 1kmabove the other granitoids in the area. This may suggest pluton construction by top-to-bottom accretion as suggested for other intrusions of the Tuscan magmatic Province (e.g. the Monte Capanne pluton; Farina et al., 2010; Barboni et al., 2015)

Overall, zircon ages vary over more than 200 ka, which precludes the calculation of a geologically meaningful weighted mean age from the entire zircon population of any of the analysed samples. Zircon crystals from MTR-22 exhibit the narrowest age dispersion among the dated samples, with eight of the eleven $^{206}Pb/^{238}U$ zircon dates overlapping within error, giving a weighted mean of 3.624 ±0.008 Ma (MSWD =1.2, Fig.5). If a single grain dated at 4.557 ±0.020 is excluded, the duration of zircon crystallization for this sample is 188 ±110 ka. The younger samples exhibit larger age dispersions, with individual rock samples from the eastern magmatic pulse characterized by timescales of zircon crystallization ranging from 279 ±59 ka to a maximum of 626 ±124ka. The eight zircon grains dated from the Roccastrada rhyolite display an age variability of 221 ±43 ka. Finally, sample Carb-C has zircon $^{206}Pb/^{238}U$ ages ranging between 3.555 ±0.005 to 1.681±0.027Ma. However, twenty out of twenty-two dates are within 1.998 ±0.027 and 1.681 ±0.014 Ma (i.e. 317±41ka).

4.5. Hf isotopic composition

We determined the Hf isotopic composition of fifty-one zircon grains. All the crystals have a distinct crustal hafnium isotope signature, with ε_{Hf}values ranging between −6.9 and −11.9 (Figs.7 and 8). In the western part of the magmatic field, the data show an overall increase in $\varepsilon_{Hf}$from the oldest to the youngest magmatic pulse: zircon grains from sample MTR-22 have homogeneous isotopic compositions, with average ε_{Hf} of −11.4 ±0.5 (1SD), while grains from sample Carb-C show significant isotopic variabil-

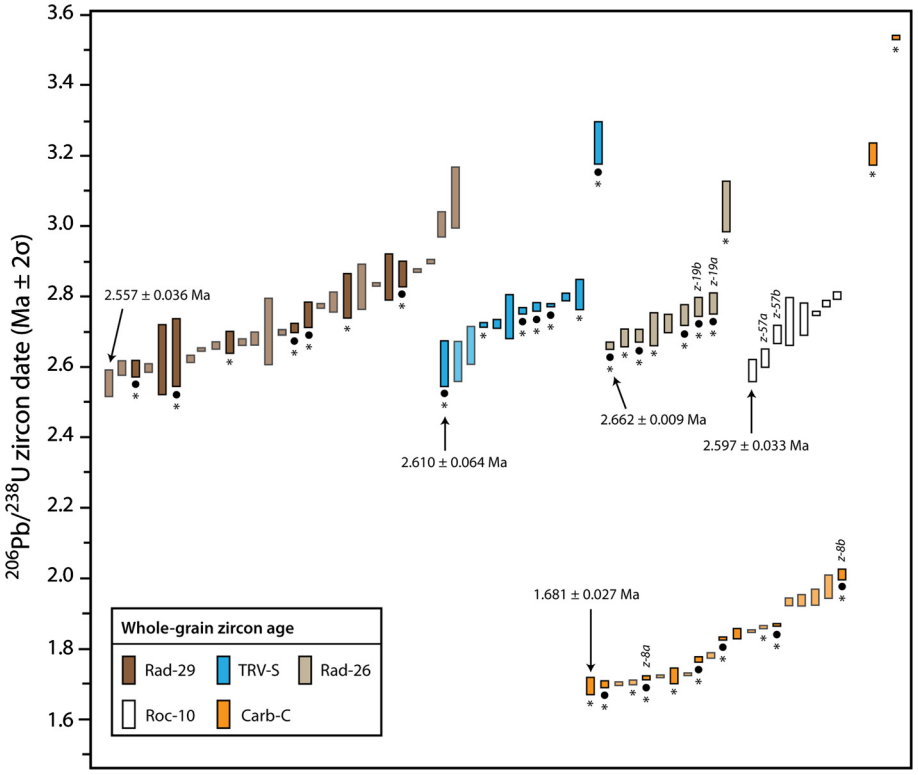

Figure 6. Rank-order plot of high-precision ID-TIMS $^{206}Pb/^{238}U$ zircon dates from three monzogranites of the Larderello-Travale intrusive system and for the Roccastrada rhyolite. Coloured rectangles are single-grain/fragments analyses with vertical lengths corresponding to 2σ uncertainties. Below the rectangles, asterisks indicate zircon grains for which bulk-grain Hf isotope were determined while black dots mark grains for which in-situ zircon oxygen analyses are available. Light-coloured rectangles are zircon that were not previously CL-imaged. For each sample, the age of the youngest dated grains is indicated. Labelled grains flag fragments from individual zircon.

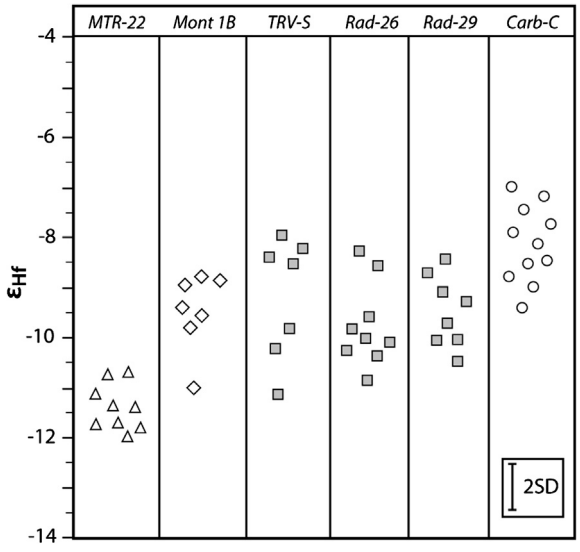

Figure 7. Hf isotope composition of zircon crystals from the Larderello-Travale granites.

ity spanning between −6.9 and −9.4 and display an average ε_{Hf} of −8.1 ±0.8 (1SD).

In the eastern part of the intrusive complex, zircon crystals from rocks formed during the second and third magmatic pulse (Mont-1B, TRV-S, Rad-26, Rad-29) show average ε_{Hf} values that are between those characterizing samples MTR-22 and Carb-C on the west. These rocks display different degrees of intra-sample Hf isotope variability (Fig.7), with grains from sample TRV-S being the most heterogeneous in $^{176}Hf/^{177}Hf$ (i.e. ε_{Hf} from −7.9 to −11.1).

5. Discussion

5.1. Genesis of the Larderello-Travale granites

Using the empirical equation proposed by Lackey et al.(2008): $\delta^{18}O_{wr} \approx \delta^{18}O_{zr} + 0.0612*(wt\%\ SiO_2) - 2.5‰$ and the oxygen isotope compositions from the Larderello-Travale granites, it is possible to estimate the oxygen isotope composition of the whole-rock ($\delta^{18}O_{wr}$), which serves as a first-order approximation of the melt $\delta^{18}O$. Considering that the silica contents of the Larderello-Travale granites range between 69 and 79 wt% (Dini et al., 2005), the calculated whole-rock $\delta^{18}O$ is ~2‰ higher than that measured in the zircon crystals. Therefore, zircon of the Larderello-Travale intrusive system crystallized from magmas with oxygen isotope compositions greater than 11‰ and strongly negative ε_{Hf} of below −7. The new data are consistent with the range of $\delta^{18}O$ (quartz, feldspars, zircon) and zircon ε_{Hf} measured in similar Tuscan granites (e.g. Gagnevin et al., 2011). These features are in good agreement with the highly peraluminous character of the monzogranites, their high whole-rock initial Sr isotopic composition (0.715-0.720) and their low ε_{Nd}(<−7; Dini et al., 2005). These lines of evidence indicate that the Larderello-Travale granites are crustally-derived magmas mostly produced by melting of isotopically heterogeneous supracrustal material. Their chemical and isotopic characteristics suggest that the main type of source involved in the genesis of these granites are aluminium-rich clastic protoliths such as the micaschists drilled from the Larderello basement (Dini et al., 2005) or other metapelitic rocks from the Tuscan basement (e.g. the Calamita schists; Sirevaag et al., 2016).

5.2. Polybaric magma storage and crystallization

The spread in U-Pb zircon ages that characterizes individual rock samples from the Larderello-Travale intrusive system

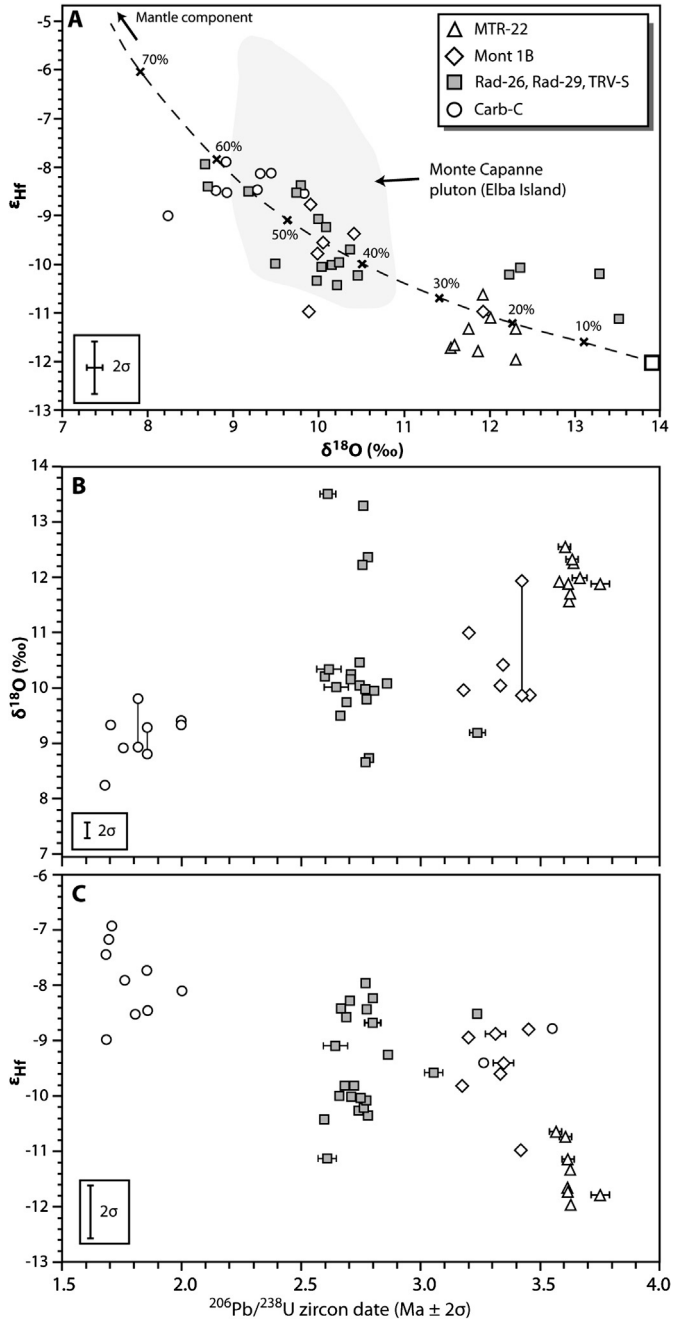

Figure 8. (A)Intercrystal oxygen and hafnium isotopic heterogeneities of Larderello-Travale zircon crystals. The grey field represents the composition of zircon crystals from intrusive rocks at Elba Island (from Gagnevin et al., 2011). The dashed line illustrates the result of a mass-balance binary-mixing model between a mantle-derived magma ($\varepsilon_{Hf}=-12$; $\delta^{18}O=14‰$) and a crustal component.The model is calculated considering a $Hf_{crust}/Hf_{mantle}=8$. (B) O-isotopiccompositions of U-Pb dated zircons; tie lines link zircon grains for which the core and rim oxygen isotopic composition was determined. (C) Hf-isotopic compositions of U-Pb dated zircons.

is consistent with an increasing number of recent zircon high-precision geochronological studies of plutonic and volcanic rocks (e.g., Samperton et al., 2015; Buret et al., 2017). For small-sized, shallow-level high-silica intrusives like the Larderello-Travale granites, thermal simulations indicate that zircon age variabilities of hundreds of thousands of years within a hand-sample cannot be the result of zircon crystallization at the emplacement level (Barboni et al., 2015). Thermal simulations have been used by Barboni et al.(2015) to calculate the time-lag between zircon saturation and complete crystallization of a granitic body emplaced in the upper crust, with the top of the pluton at 6 km depth. The models tested whether the range of zircon dates observed for the Monte Capanne pluton, a late Miocene monzogranite in the Tuscan Magmatic province, could be produced by post-emplacement cooling; i.e. a simple case in which the magma is emplaced above zircon saturation temperature and zircons are crystallized after emplacement. The result of this modelling shows that even using conservative estimates like a steep geothermal gradient of 40°C/km and multi-batch emplacement scenarios (i.e. arrival of multiple short-lived pulses), the maximum zircon crystallization time does not exceed ~70 ka. Shorter time scales of conductive cooling at the emplacement level are expected for the Larderello-Travale system since for these granites, the pluton top is located at lower depths (~4km). Also, their strongly peraluminous and high silica composition suggest that the magma was emplaced at temperatures <850°C (Clemens and Wall, 1981), ~50°C lower than the temperature implemented in the simulations of Barboni et al.(2015). Based on these data, we can conclude that the maximum zircon crystallization time at the emplacement depth for the granite of the Larderello-Travale system was at least one order of magnitude shorter than the age dispersion observed for most of the monzogranites (t =300-600 ka). Moreover, it is worth noting that CA-ID-TIMS U-Pb zircon ages are individual bulk-grain analyses in which the entire growth history of the crystal is averaged. This implies that the age spread observed between zircon crystals within individual granite samples represents a minimum estimate of the age range in the rock. Furthermore, in strongly peraluminous magmas cordierite is only stable at pressure lower than 0.5 GPa, while garnet represents the stable aluminosilicate at higher pressures (Clemens and Wall, 1981). Based on the above arguments, we conclude that most of the zircon grains from the studied granites crystallized in the middle crust, at depths between the level of emplacement and ca. 12-15 km as indicated by the occurrence of cordierite in the rock. Zircon crystals formed at depth were subsequently recycled and juxtaposed during ascent and emplacement of the magmas at shallow level. This model can efficiently explain the occurrence of isotopically-diverse crystals in the same rock volume and fulfils the portrayed idea of rapid zircon dissolution-precipitation in anatectic melts (Farina et al., 2014a). Three lines of evidence support this conclusion: i) In high-grade metapelites more than 80% of the Zr of the rock is allocated in zircon (Villaseca et al., 2007) and most of the zircon crystals are hosted in biotite that is the main reactant in melt-producing fluid-absent reactions (Bea and Montero, 1999). Therefore, during melting, zircon grains are liberated in the newly formed melt and can readily dissolve. ii) Three-dimensional modelling of zircon dissolution rates during crustal melting performed using the equation of Watson (1996) invariably suggest that zircon dissolves in hundreds or maximum few thousands of years at temperatures as low as 750°C (Bindeman and Melnik, 2016). iii) The temperature range at which biotite fluid-absent melting of Al-rich metasedimentary sources produces melt fractions that are large enough to be extracted (ca. 780-900°C, Brown, 2013) overlaps with the temperature of zircon saturation calculated using the equations of Boehnke et al.(2013) for the Larderello-Travale granite bulk rock compositions (730-850°C).

Most of the monzogranites show porphyritic textures, with phenocrysts of biotite, cordierite, quartz and feldspars hosted within a finer grained matrix made of the same rock-forming phases (Dini et al., 2005). Thus, the textural observations are in good agreement with the inference from high-precision zircon data and thermal modelling and support the idea that crystallization started in a magma reservoir located in the middle crust before final emplacement at shallow-level.

Finally, it is worth mentioning that the age spread exhibited by zircon from the monzogranites collected in the eastern part of the

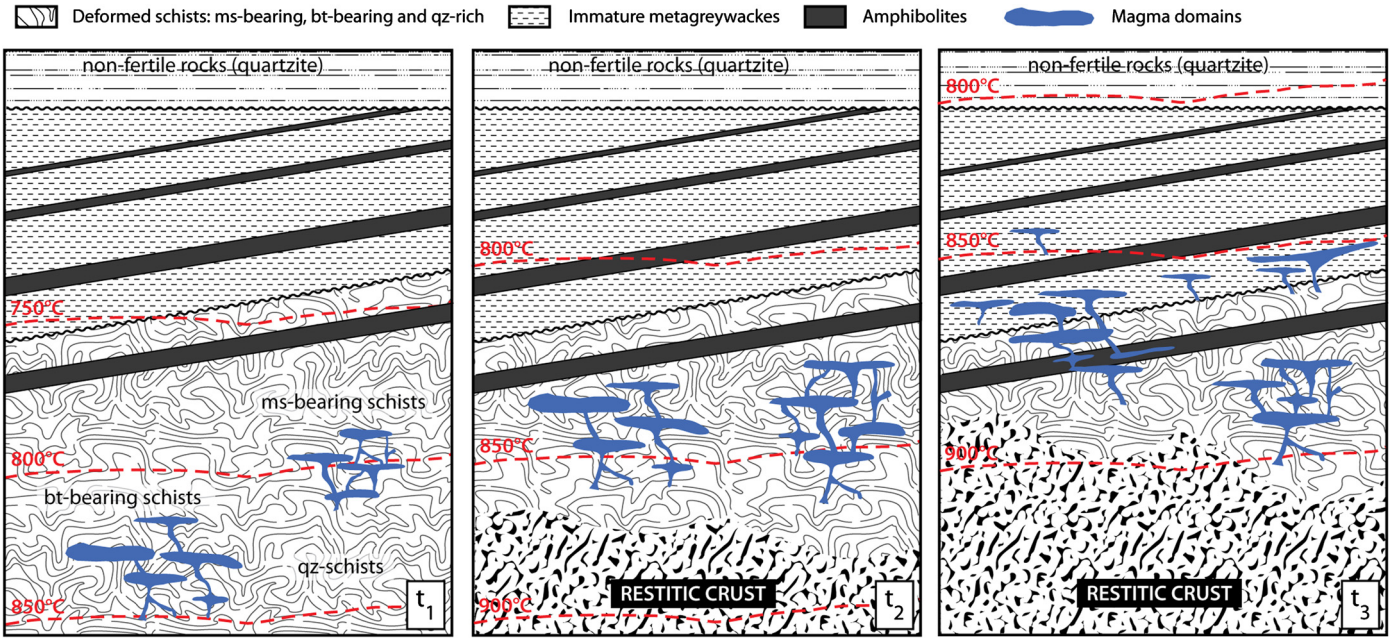

Figure 9. Sketch illustrating the formation of the Larderello–Travale magmas. The three panels (t_1–t_2–t_3) show the thermal evolution of the continental crust. The cartoon illustrates a crustal section made of different lithologies with unconformities delimiting domains of rocks with different ages. Through time, independent magma domains are formed depending on the temperature achieved in the crust and on the composition of the crustal protoliths. At t_1 and t_2 deformed metapelitic schists melt via muscovite and biotite–fluid absent melting reactions. At t_3 immature metagreywackes and volcanoclastic sequences start to melt. A minor amount of magma is also produced by the amphibolitic domains.

Larderello–Travale system (i.e. Mont–1B, TRV–S, Rad–26, Rad–29) and zircon in the Roccastrada rhyolite (Roc–10) overlap, indicating that shallow–level intrusives and rhyolites were fed by a common, compositionally heterogeneous magma reservoir that evolved for ~336 ±43 ky before emplacement or eruption (Fig.6).

5.3. Zircon crystallization in discrete melt domains

Most of the individual granitic rocks from the Larderello–Travale intrusive system contain contemporaneous zircon crystals exhibiting different $\delta^{18}O$ and ε_{Hf} isotope compositions (Fig.8), a feature that suggests co–existence of multiple and isotopically distinct magma batches at depth. The easiest way to envision such a scenario is imagining different coeval magmatic domains that are physically separated (Fig.9) and evolve mostly independently for hundreds of thousands of years (i.e. during most of the zircons crystallization history). The significant intra–grain oxygen isotope compositional variability observed for most of the crystals (>1‰) cannot be the result of crystallization at different temperatures (Bindeman, 2008)and thus indicates that the isotopic composition of the individual magma batches changed during zircon crystallization. Moreover, as indicated by the common occurrence of complex zircon CL–patterns, we suggest that episodes of magmatic zircon partial resorption and re–precipitation took place in these isolated magma domains, prior to large–scale coalescence and chemical homogenization of the magmatic system and its subsequent ascent and emplacement. This interpretation is supported by the fact that oxygen isotope spot analyses of zircon rims do not converge to a common value, as it would be expected if the rims were crystallizing from a homogeneous magma reservoir. This is well illustrated looking at core–to–rim oxygen isotope pairs from zircon grains of the second magmatic pulse (Fig.4) where no systematic patterns are observed: the oxygen isotope composition of the rims can be either lower or higher with respect to the composition in the core. The heterogeneous oxygen isotope composition exhibited by zircon rims from the Larderello–Travale granites suggest that zircon from these rocks does not record the isotopic composition of the latest magma, likely because most of zircon crystals were readily included within biotite phenocrysts (biotite hosts ~90% of the zircon inventory) and then physically isolated from the evolving magma. In conclusion, the oxygen isotope data indicate that zircon crystallized from distinct magma batches whose composition was independently changing through time, thus reflecting the open–system evolution of multiple domains of magmas.

Zircon from the oldest magmatic pulse is significantly different from the population of zircon grains in younger rocks. Grains from sample MTR–22 have simple CL zoning patterns and exhibit an overall minor age variability of 188 ±110 ky (Fig.5). These features, together with the minor oxygen and Hf isotopic variability (Fig.8) suggest that most of the zircon grains in this rock formed in an isotopically homogeneous magma reservoir.

5.4. Coeval melting of multiple crustal sources

Many studies have shown that zircon crystals from individual samples of granites and migmatites show ranges in Hf isotope composition in the order of 5–10 epsilon units (Flowerdew et al., 2006; Farina et al., 2014a, 2014b). This variability has been traditionally explained by multiple–source mixing of crustal–and mantle–derived magmas (e.g. Kemp et al., 2007). Recently, two models were put forward suggesting that the large Hf isotope variability observed in anatectic granites can arise from partial melting of individual crustal source rocks (Farina et al., 2014a; Tang et al., 2014; Chen et al., 2015). Farina et al. (2014a, 2014b) proposed that the Hf isotope variability of magmatic zircons is primarily controlled by the ε_{Hf} variability and spatial distribution of inherited zircons in the host magma. According to this model, the $^{176}Hf/^{177}Hf$ heterogeneity of the inherited zircon cargo is directly transferred to the population of magmatic crystals by rapid dissolution and zircon re–crystallization. An alternative model has been presented by Tang et al.(2014) and Chen et al.(2015). These authors suggested that the final $^{176}Hf/^{177}Hf$ of a melt is controlled by the mass balance between the low–radiogenic Hf obtained from the dissolution of inherited zircon grains and the relatively high–

radiogenic non-zircon Hf derived from other minerals that participate in the melting reaction. Both suggested processes are capable of generating magmas with contrasting Hf composition in space (Farina et al., 2014a, 2014b) and time (Tang et al., 2014; Chen et al., 2015) and might thus hold as explanation for the observed moderate ε_{Hf} variability among the zircon populations in the monzogranites of the Larderello-Travale complex. Thus, similarly to what was proposed for other crustally-derived granites, we might be tempted to conclude that the isotope diversity observed for the Larderello-Travale granites is produced by partial melting of a single source. However, the occurrence of large intra-sample $\delta^{18}O$ zircon ranges is at odds with this hypothesis. In fact, a source undergoing partial melting can only produce batches of magmas characterized by minor (~1‰) oxygen isotope variability, as the induced oxygen isotope fractionation is small at high temperatures (T>750°C; Bindeman, 2008). Thus, and except for the oldest granitoid that exhibits limited scatter in zircon $\delta^{18}O$, our coupled stable and radiogenic isotope data in zircon requires multiple sources to be involved in the production of each of the monzogranites (Fig.9).

We conclude that diverse crustal sources are contemporaneously involved in the production of the Larderello-Travale monzogranites and the isotope variability exhibited by the population of zircon grains reflects the isotopic heterogeneity of the fertile lithologies in the continental crust. This latter fact should not be surprising considering the evidence arising from fluid-absent melting experiments. These experiments have shown that crustal rocks typically yield about 30wt% of H_2O-undersaturated granitic melt at temperatures of ~900°C (e.g. Stevens et al., 1997). Accordingly, the volume of crustally-derived granitic bodies is approximately one-third of the volume of the crust involved in the melting event. Such a thick pile of rock is certainly heterogeneous being formed by complex alternation of different lithologies both vertically and laterally as data from the Tuscan Paleozoic basement confirm. In fact, field data from the poorly exposed basement and drilled cores from the Larderello geothermal field reveal the occurrence of a complex tectonic stack made of different fertile lithologies such as micaschists, metagreywackes, gneisses and minor bodies of amphibolites and metabasites (Pandeli et al., 1994).

5.5. Isotope evolution during crustal thermal maturation

Negative correlation between $\delta^{18}O$ and ε_{Hf} was found among the populations of zircon crystals from the six monzogranites (Fig.8A). In the western part of the Larderello-Travale complex two separate magma pulses can be recognized, one formed at ~3.6Ma the other is approximately two million years younger (MTR-22 and Carb-C, respectively). Zircon crystals from these rocks, which are sampled only two km apart, display contrasting oxygen and hafnium isotope compositions (Figs.4, 7), with zircon from MTR-22 having high $\delta^{18}O$ (~12‰) and low ε_{Hf}(~−11) and those from Carb-C characterized by low $\delta^{18}O$ (~9‰) and high ε_{Hf} (~−8; Fig.8). The occurrence of this isotopic trend might suggest that mixing between mantle-and metasedimentary-derived magmas played a role in generating the covariant $\delta^{18}O$-ε_{Hf} zircon array, as convincingly suggested for other intrusive bodies and magmatic suites (e.g. Kemp et al., 2007). Although the possibility of a minor involvement of mantle-derived magmas in the genesis of the youngest magmatic pulse of the Larderello-Travale intrusive system cannot be ruled out, we consider it very unlikely for three reasons. Firstly, the major element composition of sample Carb-C matches the composition of leucosomes and experimental melts derived from metasedimentary crustal sources (Dini et al., 2005; Gao et al., 2016). Secondly, in comparison with other granites in the Tuscan Magmatic Province, none of the Larderello-Travale granites show any petrographic features supporting a mantle-derived component in their genesis, such as mafic microgranular enclaves, amphibole clots and anorthite-rich plagioclase cores. Finally, mixing calculations between a mantle-derived magma (ε_{Hf}=14; $\delta^{18}O$=5.3‰) and a crustally-derived melt(ε_{Hf}=−12; $\delta^{18}O$ =14‰) performed considering Hf_{crust}/Hf_{mantle} ranging between 3 and 8, show that the lowest $\delta^{18}O$ and highest ε_{Hf} magma composition would require addition of at least 50% of a magma derived by melting of a depleted mantle source. This result is at odds with the K_2O-rich and peraluminous character of the granites and, more importantly, it fails in accounting for the crustal Sr and Nd isotope signature of sample Carb-C (i.e. $^{87}Sr/^{86}Sr$ =0.720; ε_{Nd}=−9; Dini et al., 2005).

We propose that the $\delta^{18}O$-ε_{Hf} evolution observed for the whole Larderello-Travale intrusive system and in particular in the western sector of the magmatic field (Fig.8) reflects partial melting of compositionally different crustal source domains at progressively higher temperatures. In essence, we suggest that the overall decrease in $\delta^{18}O$ and increase in ε_{Hf} observed from the oldest to the youngest magmatic pulse represents a compositional evolution originating from the interplay between advancing geotherms in the crust and the nature of the crustal lithologies involved in the melting process. Partial melting experiments and thermodynamic simulations predict that in the absence of free-aqueous fluid in the crust, the first magmas to be produced are formed under upper-amphibolite-facies conditions by partial melting of metasedimentary rocks that had a significant fraction of Al-rich clays in their protoliths through muscovite fluid-absent reactions (~750°C; e.g. Patiño Douce and Harris, 1998). At higher temperatures (~800°C), metapelites will also start melting by incongruent reactions involving the breakdown of biotite (e.g. Pickering and Johnston, 1998). Magma batches derived from these clay-rich protoliths will form granitoids characterized by high $\delta^{18}O$ and low ε_{Hf} compositions. The high $\delta^{18}O$ of the magma reflects the high oxygen isotope composition characterizing metasedimentary Al-rich clastic rock (Bindeman, 2008)while its low $^{176}Hf/^{177}Hf$ is derived through dissolution and re-crystallization from the Hf isotopic composition of old detrital zircon crystals, which in the Larderello-Travale granites are preserved as inherited cores. Melting of this type of sources can explain the composition of zircon from sample MTR-22 as well as the general chemical features characterizing the whole Larderello-Travale system (Fig.9).

When the temperature in the source region increases ~850°C, different protoliths such as igneous rocks, andesitic lavas and immature clastic sediments can start to melt through fluid-absent melting reactions involving the breakdown of biotite and eventually amphibole (e.g. Clemens et al., 2011). The oxygen isotope composition of magmas derived from these protoliths is expected to be lower in $\delta^{18}O$ than the composition of magmas formed by partial melting of clay-rich pelites reflecting the lower $\delta^{18}O$ of immature greywackes and andesites with respect to Al-rich clastic rocks (Fig.1 in Bindeman, 2008). Immature greywackes and volcanoclastic protoliths are likely to be characterized by zircon ages close to the age of deposition of the sediment while mature metapelites commonly contain populations of detrital zircon grains with old ages. In the Tuscan basement an example of these contrasting behaviours can be observed comparing the distribution of detrital zircon ages of the Monte Calamita Schist with that of the overlying Capo d'Arco Schist (Sirevaag et al., 2016). Zircon ages spanning between 2700 and 500 Ma characterize the former, with main peaks at ~2500, 990, 780 and 610 Ma. On the contrary, zircon grains from the Capo d'Arco Schist show a unimodal age distribution with peak at ~450 Ma. The different detrital zircon age spectra characterizing contrasting sources will have an impact on the Hf isotope composition of the melts deriving from these sources and ultimately on the ε_{Hf} of magmatic zircon grains crystallized from these melts. Dissolution of old detrital zir-

con generates melts with strongly negative ε_{Hf} compositions while younger zircon grains produce melts with higher $^{176}Hf/^{177}Hf$ and thus less negative ε_{Hf} values. Biotite fluid-absent partial melting experiments conducted on large range of source compositions suggest that major-element evidence of magma mixing between melts derived by different supracrustal protoliths is likely to be cryptic. In fact, when the temperature of melting is <1000°C, the compositions of experimental melts derived by partial melting of sources spanning in composition from K-rich metapelites to relatively Na-rich greywackes and tonalities are very similar (Gao et al., 2016). Thus evidence of involvement of multiple sources in the genesis of granitic rocks can be only recorded at the mineral-scale.

When the temperature in the continental crust reaches ~900°C, magmas will also be produced by partial melting of amphibole-bearing basaltic/andesitic sources through reactions that involve the breakdown of amphibole (e.g. Rushmer, 1991). In the Tuscan basement, these protoliths commonly occur as metabasites and amphibolite layers hosted within metagreywacks and gneisses (Pandeli et al., 1994). Fluid-absent melting of a juvenile mafic crust at temperatures <950°C give rise to intermediate to felsic melts (e.g. Gao et al., 2016) that would have mantle-like oxygen isotope composition and $^{176}Hf/^{177}Hf$ that depends on the composition of the mantle from which the basaltic magmas was extracted and on the age of formation of the juvenile crust. In the genesis of the Larderello-Travale younger intrusions, a limited contribution of magmas formed by melting juvenile mafic material is possible and can be partly responsible for the shift of the isotopic composition of the granite towards lower $\delta^{18}O$ and higher ε_{Hf} values.

It is worth noting that in the Tuscan Magmatic Province thermal maturation and partial melting of crustal sources with progressively different composition have been proposed to account for the chemical and isotopic evolution of the western Elba Island magmatic complex (Farina et al., 2012,2014b). In the western Elba case, the late stage evolution of the intrusive complex involved minor hybridization with mantle-derived magmas resulting in the late emplacement of a swarm of dikes crosscutting the entire magmatic complex (Farina et al., 2012). Similar late arrival of hybrid mantle magmas characterizes all granite complexes in Tuscany (Eastern Elba, Giglio, Campiglia). We propose that the hybrid late stage evolution of the western Elba Island magmatic complex might be regarded as a possible analogue for current and future magmatic activity of the Larderello-Travale complex.

6. Conclusion

In the Larderello-Travale area, peraluminous high-silica monzogranitic magmas were emplaced at shallow-level in four main magmatic pulses. The petrochronological approach implemented in this study has provided insights into the timescale and mechanism of formation of anatectic granites:

1. Zircon grains from individual rock samples crystallized from coeval, isotopically-distinct and physically separated magma domains. The isotopic composition of these independent domains of magma changed through time by recharge with new magmas which, in some cases, caused episodes of zircon partial resorption and re-precipitation.

2. The monzogranites are mostly produced by partial melting of Al-rich clastic metasediments. However, each of the monzogranites formed through mixing of crustal magma batches derived by melting of different source rocks, with this feature reflecting the inherent heterogeneous nature of the continental crust. Crustal heterogeneity is transferred to granitic magmas and preserved at the crystal-scale.

3. The overall $\delta^{18}O$-ε_{Hf} evolution observed for the monzogranites reflects the advance of geotherms in the continental crust. The high $\delta^{18}O$ low ε_{Hf} composition of metapelite-derived magmas mixes progressively with the composition of magmas formed at higher temperatures by partial melting of non-pelitic metasediments and metaigneous sources.

4. High precision U-Pb dates point to a long-lived magmatic system in which crustal melting and melt residence in the middle crust lasted for hundreds of thousands of years before magma ascent and emplacement in the upper crust, with magma delivered in pulses.

References

Agostinetti, N.P., Licciardi, A., Piccinini, D., Mazzarini, F., Musumeci, G., Saccorotti, G., Chiarabba, C., 2017. Discovering geothermal supercritical fluids: a new frontier for seismic exploration. Sci. Rep.7, 14592.

Barboni, M., Schoene, B., 2014. Short eruption window revealed by absolute crystal growth rates in a granitic magma. Nat. Geosci.7, 524-528.

Barboni, M., Annen, C., Schoene, B., 2015. Evaluating the construction and evolution of upper crustal magma reservoirs with coupled U/Pb zircon geochronology and thermal modeling: a case study from the Mt. Capanne pluton (Elba, Italy). Earth Planet. Sci. Lett.432, 436-448.

Bea, F., Montero, P., 1999. Behavior of accessory phases and redistribution of Zr, REE, Y, Th, and U during metamorphism and partial melting of metapelites in the lower crust: an example from the Kinzigite Formation of Ivrea-Verbano, NW Italy. Geochim. Cosmochim. Acta63, 1133-1153.

Bertini, G., Casini, M., Gianelli, G., Pandeli, E., 2006. Geological structure of a long living geothermal system, Larderello, Italy. Terra Nova18, 163-169.

Bindeman, I.N., 2008. Oxygen isotopes in mantle and crustal magmas as revealed by single crystal analysis. In: Putirka, K.D., Tepley, F.J., III (Eds.), Minerals, Inclusions and Volcanic Processes. In: Reviews in Mineralogy and Geochemistry, vol.69. Mineralogical Society of America and Geochemical Society, pp.445-478.

Bindeman, I.N., Melnik, O.E., 2016. Zircon survival, rebirth and recycling during crustal melting, magma crystallization, and mixing based on numerical modelling. J. Petrol.57 (3), 437-460.

Boehnke, P., Watson, E.B., Trail, D., Harrison, T.M., Schmitt, A.K., 2013. Zircon saturation re-revisited. Chem. Geol.351, 324-334.

Brown, M., 2013. Granite: from genesis to emplacement. Geol. Soc. Am. Bull.125, 1079-1113.

Buret, Y., Wotzlaw, J-F., Roozen, S., Guillong, M., von Quadt, A., Heinrich, C.A., 2017. Zircon petrochronological evidence for a plutonic-volcanic connection in porphyry copper deposits. Geology45, 623-626. https://doi.org/10.1130/G38994.1.

Cashman, K.V., Sparks, R.S.J., Blundy, J.D., 2017. Vertically extensive and unstable magmatic systems: a unified view of igneous processes. Science355, 6331. https://doi.org/10.1126/science.aag3055.

Chen, Y-X., Gao, P., Zheng, Y-F., 2015. The anatectic effect on the zircon Hf isotope composition of migmatites and associated granites. Lithos238, 174-184.

Clemens, J.D., Wall, V.J., 1981. Origin and crystallization of some peraluminous (S-type) granitic magmas. Can. Mineral.19, 111-131.

Clemens, J.D., Stevens, G., Farina, F., 2011. The enigmatic sources of I-type granites: the peritectic connexion. Lithos126, 174-181.

Clemens, J.D., Stevens, G., 2012. What controls chemical variation in granitic magmas? Lithos, 134-135, 317-329.

Dini, A., Gianelli, G., Puxeddu, M., Ruggieri, G., 2005. Origin and evolution of Pliocene-Pleistocene granites from the Larderello geothermal field (Tuscan Magmatic Province, Italy). Lithos81, 1-31.

Farina, F., Dini, A., Innocenti, F., Rocchi, S., Westerman, D.S., 2010. Rapid incremental assembly of the Monte Capanne pluton (Elba Island, Tuscany) by downward stacking of magma sheets. Geol. Soc. Am. Bull.122, 1463-1479.

Farina, F., Stevens, G., Dini, A., Rocchi, S., 2012. Peritectic phase entrainment and magma mixing in the late Miocene Elba Island laccolith-pluton-dyke complex (Italy). Lithos153, 243-260.

Farina, F., Stevens, G., Gerdes, A., Frei, D., 2014a. Small-scale Hf isotopic variability in the Peninsula pluton (South Africa): the processes that control inheritance of source $^{176}Hf/^{177}Hf$ diversity in S-type granites. Contrib. Mineral. Petrol.168, 1-18.

Farina, F., Dini, A., Rocchi, S., Stevens, G., 2014b. Extreme mineral-scale Sr isotope heterogeneity in granites by disequilibrium melting of the crust. Earth Planet. Sci. Lett.399, 103-115.

Flowerdew, M.J., Millar, I.L., Vaughan, A.P.M., Horstwood, M.S.A., Fanning, C.M., 2006. The source of granitic gneisses and migmatites in the Antarctic Peninsula: a combined U-Pb SHRIMP and laser ablation Hf isotope study of complex zircons. Contrib. Mineral. Petrol.151, 751-768.

Gagnevin, D., Daly, J.S., Horstwood, M.S.A., Whitehouse, M.J., 2011. In-situzircon U-Pb, oxygen and hafnium isotopic evidence for magma mixing and mantle metasomatism in the Tuscan Magmatic Province, Italy. Earth Planet. Sci. Lett.305, 45-56.

Gao, P., Zheng, Y-F., Zhao, Z-F., 2016. Experimental melts from crustal rocks: a lithochemical constraint on granite petrogenesis. Lithos266-267, 133-157.

Gianelli, G., Manzella, A., Puxeddu, M., 1997. Crustal models of southern Tuscany (Italy). Tectonophysics281, 221–239.

Hawkesworth, C., Cawood, P.A., Dhuime, B., 2018. Rates of generation and growth of the continental crust. Geosci. Front. https://doi.org/10.1016/j.gsf.2018.02.004. Inpress.

Kemp, A.I.S., Hawkesworth, C.J., Foster, G.L., Paterson, B.A., Woodhead, J.D., Hergt, J.M., Gray, C.M., Whitehouse, M.J., 2007. Magmatic and crustal differentiation history of granitic rocks from Hf–O isotopes in zircon. Science315, 980–984.

Malinverno, A., Ryan, W.B.F., 1986. Extension in the Tyrrhenian Sea and shortening in the Apennines as a result of arc migration driver by sinking of the lithosphere. Tectonics5, 227–245.

Lackey, J.S., Valley, J.W., Chen, J.C., Stockli, D.F., 2008. Dynamic magma systems, crustal recycling, and alteration in the Central Sierra Nevada Batholith: the oxygen isotope record. J. Petrol.49, 1397–1426.

Lustrino, M., Duggen, S., Rosemberg, C.L., 2011.The Central–Western Mediterranean: anomalous igneous activity in an anomalous collisional tectonic setting. Earth-Sci. Rev.104, 1–40.

Pandeli, E., Gianelli, G., Puxeddu, M., Elter, F.M., 1994. The Paleozoic Basement of the Northern Apennines: stratigraphy, tectono–metamorphic evolution and Alpine hydrothermal processes. Mem. Soc. Geol. Ital.48, 627–654.

Paoli, G., Stokke, H.H., Rocchi, S., Sirevaag, H., Ksienzyk, A.K., Jacobs, J., Košler, J., 2016. Basement provenance revealed by U–Pb detrital zircon ages: a tale of African and European heritage in Tuscany, Italy. Lithos277, 376–387.

Patiño Douce, A.E., Harris, N., 1998. Experimental constraints on Himalayan anatexis. J. Petrol.39, 689–710.

Petford, N., Cruden, A.R., McCaffrey, K.J.W., Vigneresse, J.–L., 2000. Granite magma formation, transport and emplacement in the Earth's crust. Nature408, 669–673.

Pickering, J.M., Johnston, D.A., 1998. Fluid–absent melting behaviour of a two mica metapelite: experimental constraints on the origin of Black Hill Granite. J. Petrol.39 (10), 1787–1804.

Pinarelli, L., Poli, G., Santo, A., 1989. Geochemical characterization of recent volcanism from the Tuscan Magmatic Province (Central Italy): the Roccastrada and San Vincenzo centers. Period. Mineral.58, 67–96.

Rushmer, T., 1991. Partial melting of two amphibolites: contrasting experimental results under fluid–absent conditions. Contrib. Mineral. Petrol.107, 41–59.

Samperton, K.M., Schoene, B., Cottle, J.M., Keller, C.B., Crowley, J.L., Schmitz, M.D., 2015. Magma emplacement, differentiation and cooling in the middle crust: integrated zircon geochronological–geochemical constraints from the Bergell Intrusion, Central Alps. Chem. Geol.417, 322–340. https://doi.org/10.1016/j.chemgeo.2015.10.024.

Schaltegger, U., Schmitt, A.K., Horstwood, M.S.A., 2015. U–Th–Pb zircon geochronology by ID–TIMS, SIMS, and laser ablation ICP–MS: recipes, interpretations, and opportunities. Chem. Geol.402, 89–110.

Schmitt, A.K., Klitzke, M., Gerdes, A., Schäfer, C., 2017. Zircon hafnium–oxygen isotope and trace element petrochronology of intraplate volcanic rocks from the Eifel (Germany) and implications for mantle versus crustal origins of zircon megacrysts. J. Petrol.58 (9), 1841–1870.

Sirevaag, H., Jacobs, J., Ksienzyk, A.K., Rocchi, S., Paoli, G., Jørgensen, H., Košler, J., 2016. From Gondwana to Europe: the journey of Elba Island (Italy) as recorded by U–Pb detrital zircon ages of Paleozoic metasedimentary rocks. Gondwana Res.38, 273–288.

Stevens, G., Clemens, J.D., Droop, G.T.R., 1997. Melt production during granulite–facies anatexis: experimental data from "primitive" metasedimentary protoliths. Contrib. Mineral. Petrol.128, 352–370.

Szymanowski, D., Ellis, B.S., Bachmann, O., Guillong, M., Phillips, W.M., 2015. Bridging basalts and rhyolites in the Yellowstone–Snake River Plain volcanic province: the elusive intermediate step. Earth Planet. Sci. Lett.415, 80–89.

Tang, M., Wang, X.–L., Shu, X.–J., Wang, D., Yang, T., Gopon, P., 2014. Hafnium isotopic heterogeneity in zircons from granitic rocks: geochemical evaluation and modelling of "zircon effect" in crustal anatexis. Earth Planet. Sci. Lett.389, 188–199.

Valley, J.W., Kinny, P.D., Schulze, D.J., Spicuzza, M.J., 1998. Zircon megacrysts from kimberlite: oxygen isotopevariability among mantle melts. Contrib. Mineral. Petrol.133, 1–11.

Villa, I., Ruggieri, G., Puxeddu, M., Bertini, G., 2006. Geochronology and isotope transport systematics in a subsurface granite from the Larderello–Travale geothermal system (Italy). J. Volcanol. Geotherm. Res.152, 20–50.

Villaseca, C., Orejana, D., Paterson, B.A., 2007. Zr–LREE rich minerals in residual peraluminous granulites, another factor in the origin of low Zr–LREE granitic melts? Lithos96, 3–4. 375–386.

Watson, E.B., 1996. Dissolution, growth and survival of zircons during crustal fusion: kinetic principles, geological models and implications for isotopic inheritance. Trans. R. Soc. Edinb. Earth Sci.87, 43–56.

Wotzlaw, J.–F., Schaltegger, U., Frick, D.A., Dungan, M.A., Gerdes, A., Günther, D., 2013. Tracking the evolution of large–volume silicic magma reservoirs from assembly to supereruption. Geology41, 867–870. https://doi.org/10.1130/G34366.1.

Wotzlaw, J.F., Bindeman, I.N., Watts, K.E., Schmitt, A.K., Caricchi, L., Schaltegger, U., 2014. Linking rapid magma reservoir assembly and eruption trigger mechanisms at evolved Yellowstone–type supervolcanoes. Geology42, 807–810.